J Mater Sci (2015) 50:4160–4173
DOI 10.1007/s10853-015-8841-3

Influence of Zn interlayer addition on microstructure and mechanical properties of friction stir welded AZ31 Mg alloy

R. Z. Xu · D. R. Ni · Q. Yang · C. Z. Liu · Z. Y. Ma

Received: 10 November 2014 / Accepted: 5 January 2015 / Published online: 23 January 2015

Abstract 2.4-mm-thick AZ31 Mg alloy sheets were friction stir spot welded without and with the addition of Zn interlayers ranging from 0.04 to 0.16 mm in thickness. For the joints without Zn interlayers, although the loads of the joints could be increased by changing the end surface geometry and size of the shoulders, the small bonded area and hook defects limited further increase of joint loads. For the joints with Zn interlayers, the Zn interlayer reacted with the Mg substrate, forming a Mg–Zn brazed zone composed of complex Mg–Zn intermetallics and a thin strip of (α-Mg + MgZn) eutectoid structure, thereby increasing the bonded area and reducing the hook defects of joints at the same time. As a result, the maximum joint load increased from 2.7 to 5.2 kN using a 10-mm-diameter concave shoulder with a 0.12-mm-thick Zn interlayer. A thicker interlayer resulted in a significant increase in the thickness of the thin strip in the hook region, and a thinner interlayer led to the formation of more defects due to intense diffusion reactions, thereby reducing the joint loads.

Introduction

Friction stir spot welding (FSSW) is a variant of friction stir welding [1, 2]. As an emerging solid-state joining method, FSSW presents great potential in substituting conventional resistance spot welding and riveting in joining lightweight structural metals for the automotive and aerospace industries [3, 4]. Mg alloys are known as excellent candidates for lightweight structural materials due to their low density, high specific strength, and acceptable ductility [5]. Therefore, there is much interest in the FSSW of Mg alloys for their ability to provide weight reduction [6].

In general, the temperature attained during FSSW is lower than the melting point of base materials, so FSSW is free of defects commonly associated with fusion welding [7]. However, a lot of studies have proven that the formation of special hook defects (Fig. 1a) decreased the load of FSSW joints significantly [8]. It was suggested that during FSSW, the heated and softened material underneath the shoulder first moved toward the pin root and then moved along the pin surface downward as a result of the dragging force of the rotating threads. Once the material arrived at the pin tip, it was forced upward and outward, and then it moved back toward the pin following a helical rotational path [9–11]. At last, the different hook curves formed due to the effect of heat generation and material flow. It should be pointed out that the material flow during FSSW is quite complex and not fully understood at present [12].

Many attempts have been made to increase the loads of FSSW Mg alloy joints. For example, some work focused on changing the size and shape of hook defects by optimizing the welding parameters [7, 8, 13]. In addition, the optimization of tool geometry is an important method of changing the dimensions and curvatures of hooks, but the theoretical concept for the tool design has not yet been established [14]. Only limited research has been reported concerning the effect of pin shape on the mechanical

R. Z. Xu · D. R. Ni · Q. Yang · Z. Y. Ma (✉)
Shenyang National Laboratory for Materials Science, Institute of Metal Research, Chinese Academy of Sciences, 72 Wenhua Road, Shenyang 110016, China
e-mail: zyma@imr.ac.cn

R. Z. Xu · C. Z. Liu
College of Material Science and Engineering, Shenyang Aerospace University, 37 Daoyi South Street, Shenyang 110136, China

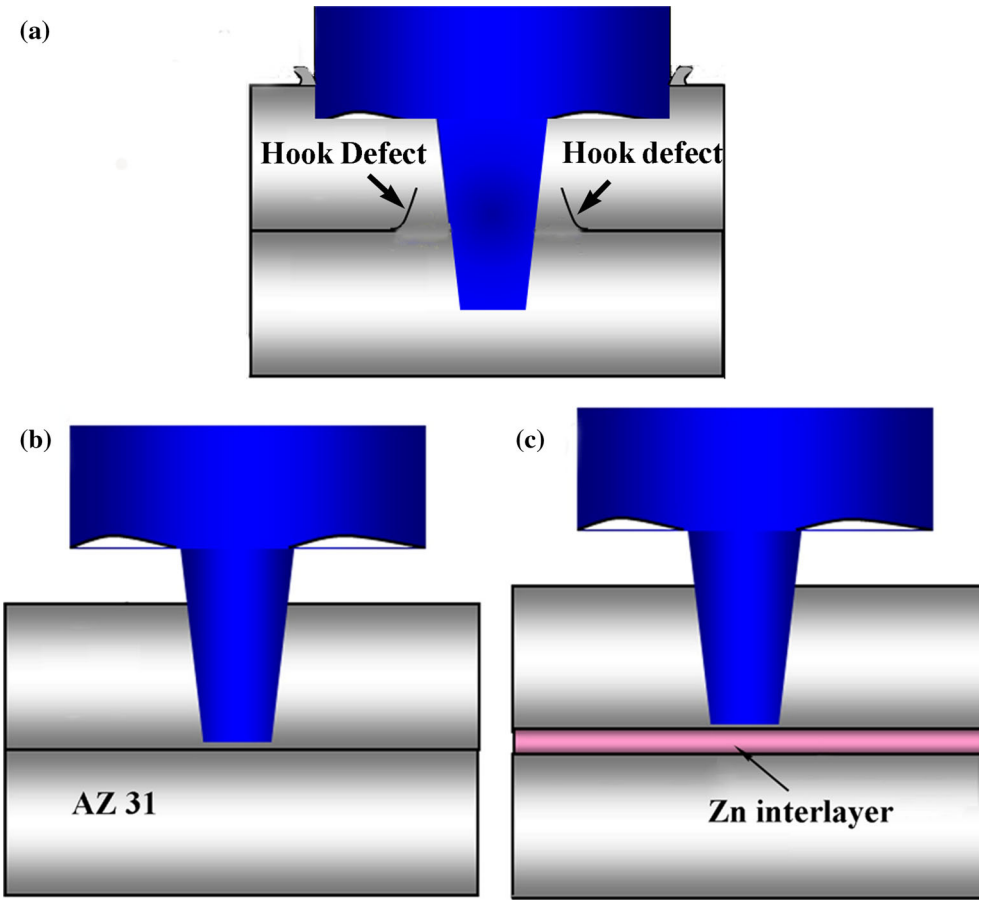

Fig. 1 Schematic of **a** hook defects in the FSSW joint and AZ31 FSSW **b** without and **c** with the addition of Zn interlayer

properties of FSSW Mg alloy joints [15]. In fact, during FSSW, the effect of shoulder shape and size on heat generation and material flow should not be neglected, but related investigations on Mg alloys are lacking [16].

Furthermore, some studies tried to increase the area of the bonded zone using improved FSSW processes, such as bonding-FSSW and FSSW with a heating process [17–19]. For bonding-FSSW, the area of the bonded zone of the joints was increased by adhesives, so the load of the joints could be improved [20]. However, the aging and poor high-temperature performance of adhesives should not be ignored. For the FSSW with a heating process, the width of the bonded zone was increased by heating the AZ31 Mg alloy joints during FSSW [21]. However, the troublesome operation would limit the wide applications of this process. In fact, the above two hybrid technologies only increased the area of the bonded zone, but could not avoid the appearance of hook defects. Therefore, new processes are still needed for eliminating the hook defects in FSSW Mg alloy joints and increasing the area of the bonded zone simultaneously.

Due to the short heating time and the low heat input, FSSW is more energy efficient and clean than other spot welding techniques [22]. However, the low welding temperature would increase the difficulty of solid state bonding between the top and bottom sheets, resulting in the formation of more voids, a wider non-contact zone, and a partial metallurgical zone in the FSSW joints [18, 20, 21]. The increase in holding time may cause the welding temperature of the FSSW joints to increase quickly at the initial stage, but the decrease in the friction force between sheets and tool results in an obvious decrease in the rate of temperature increase at subsequent stages [19]. In addition, increasing the rotational rate could also increase the heat input remarkably, but would cause a higher residual stress [22].

Furthermore, increasing the welding temperature promotes easily the formation of an oxide film of faying surface between the top and bottom Mg sheets, which is not beneficial to the elimination of hook defects [14, 17]. Therefore, under the condition of insufficient heat input, decreasing the reaction temperature at the interface may be a potential method of promoting the interface bonding and avoiding hook defects.

It is well known that adding solder alloys is an important way to reduce interface reaction temperature [23, 24]. Zn, as an economic and innoxious solder metal, is effective in promoting the bonding of Mg alloys [24, 25]. In FSSW, the

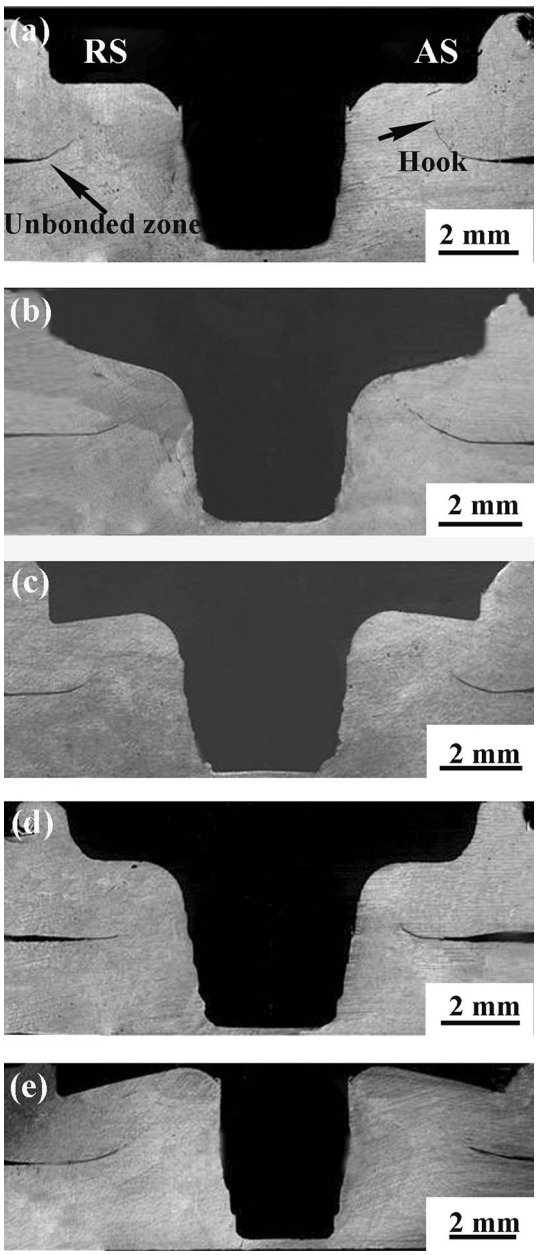

Fig. 2 Typical cross-section photographs of FSSW AZ31 Mg alloy joints using different shoulders: **a** flat, Φ10; **b** convex, Φ10; **c** concave, Φ10; **d** concave, Φ8; and **e** concave, Φ12

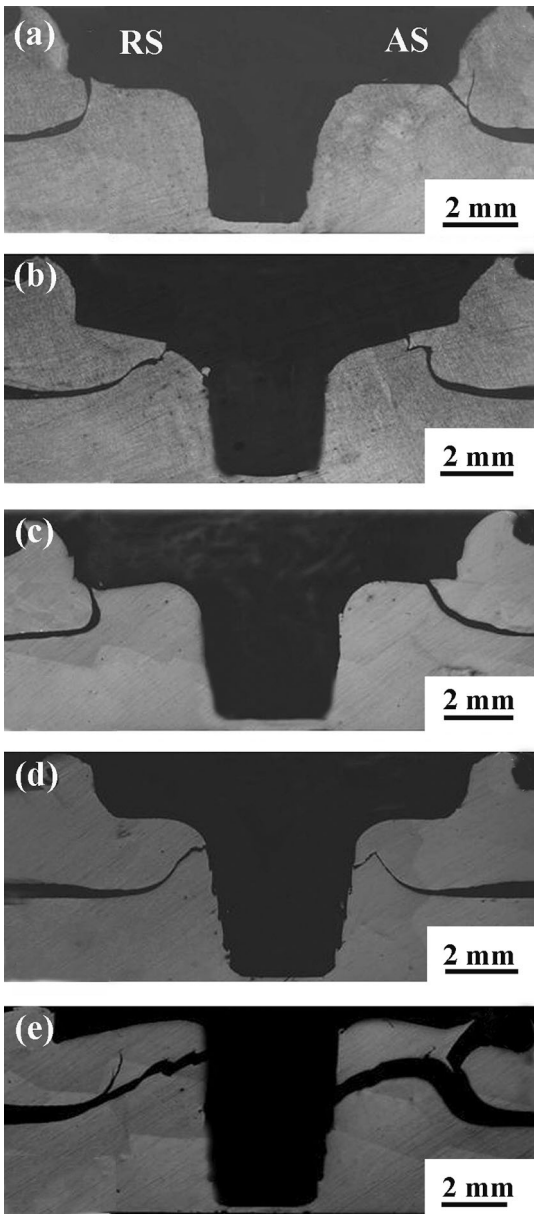

Fig. 3 Typical fracture locations of FSSW AZ31 Mg alloy joints using different shoulders: **a** flat, Φ10; **b** convex, Φ10; **c** concave, Φ10; **d** concave, Φ8; and **e** concave, Φ12

welding process could provide the pressure, reaction temperature, and time for the diffusion reaction of Mg and Zn due to the action of rotation, plunge, and keeping (dwell time) of the stir tool. Therefore, adding a Zn interlayer may be beneficial for joining of the Mg sheets and increasing the area of the bonded zone, thereby improving the mechanical properties of the FSSW joints.

In this study, the Zn interlayers with different thicknesses were selected for the FSSW of AZ31 Mg alloy with the goal of eliminating hook defects and increasing the area of the bonded zone at the same time, thereby increasing the tensile-shear load of the joints. In addition, the influencing mechanism of the Zn interlayer addition on the microstructure and mechanical properties of the joints was investigated in detail.

Experimental

2.4-mm-thick AZ31 Mg sheets with a composition of Mg–3.02Al–0.82Zn–0.30Mn–0.01Si (wt%) were used in this

study. All the FSSW operations with and without the interlayer were conducted at a tool rotational rate of 3000 rpm and a plunge rate of 2.5 mm/s using a taper threaded pin (M4, 7.5°) 3.8 mm in length. The tool withdrawing rate was 30 mm/s at the end of each spot welding operation and the dwell time was 5 s. For the FSSW without the addition of a Zn interlayer, Mg alloy sheets were welded with different shoulder end surfaces (flat, concave and convex) and shoulder sizes (Φ8, Φ10 and Φ12 mm). For the FSSW with the addition of a Zn interlayer, Zn interlayers with different thicknesses (0.04, 0.08, 0.12, and 0.16 mm) were added between two welded Mg sheets prior to the welding operation. Then, FSSW was conducted using a 10-mm-diameter concave shoulder. The schematic of the FSSW process without and with the addition of a Zn interlayer is shown in Fig. 1b, c.

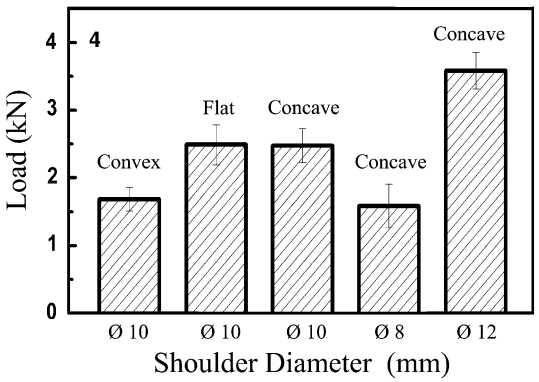

Fig. 4 Tensile-shear loads of FSSW AZ31 joints using different shoulders

Specimens for microstructure examinations were sectioned through the center of the joints and parallel to the loading direction. After being mechanically ground and polished, the specimens were etched with an etching reagent consisting of 4.2 g picric acid, 10 ml acetic acid, 10 ml H_2O, and 70 ml ethanol. Microstructures were examined by optical microscope (OM), scanning electron microscope (SEM, LEO Supra 35) with an energy-dispersive X-ray dispersive spectrometer (EDS, Oxford Instruments X-Max), and transmission electron microscope (TEM, FEI Tecnai F20) equipped with an energy-dispersive X-ray spectrometer (EDS, Oxford Instruments INCA). The beam size used in the EDS spectroscopy data selection of TEM was in the range of 10–20 nm, and the "Multi-Polynomial" is used as a background model.

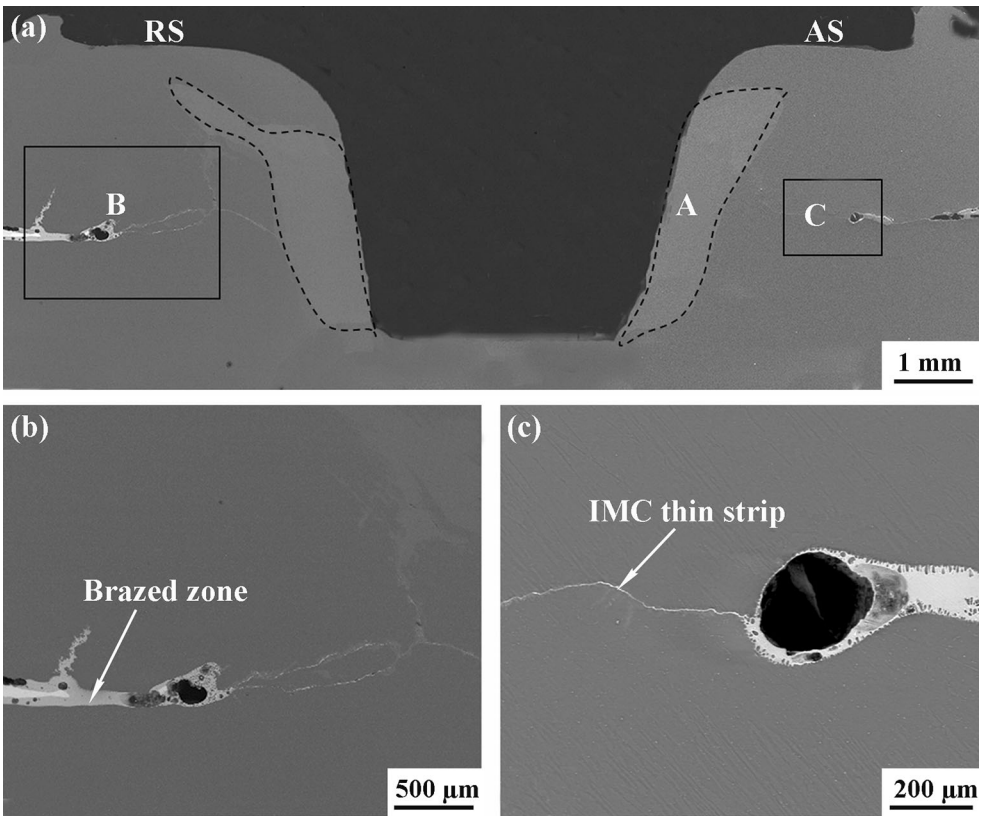

Fig. 5 **a** Typical cross-section photograph of FSSW AZ31 joint with an addition of 0.04-mm-thick Zn interlayer and the microstructures of **b** region B and **c** region C

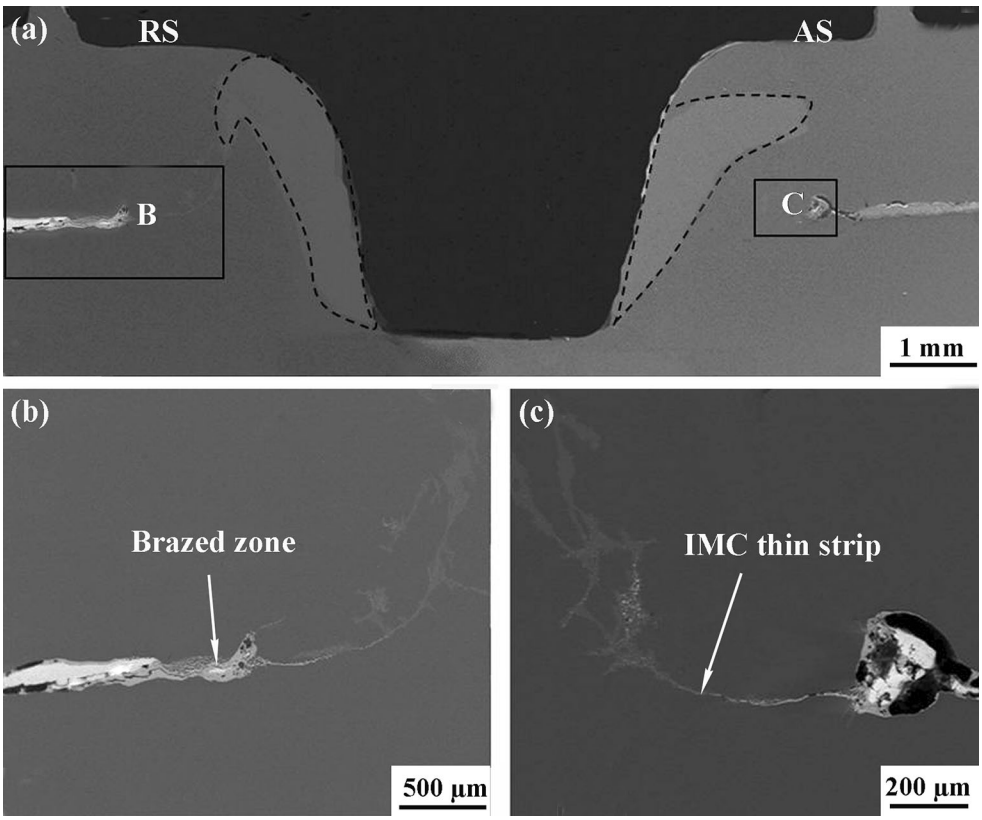

Fig. 6 **a** Typical cross-section photograph of FSSW AZ31 joint with an addition of 0.08-mm-thick Zn interlayer and the microstructures of **b** region B and **c** region C

The lap-shear specimens with a length of 100 mm, a width of 30 mm, and a 30 × 30-mm overlap area were electrical discharge machined from the FSSW joints. The lap-shear tensile tests were conducted using a Zwick/Roell Z050 tester at a tensile speed of 1 mm/min. The property values for each condition were calculated by averaging three test results. The fracture location and characteristics were examined using OM and SEM.

Results

Macrostructure and properties of FSSW AZ31 joints without the addition of Zn interlayer

Figure 2 shows the typical cross section photographs of FSSW AZ31 Mg alloy joints using different shoulders. Hook defects were detected on both the advancing side (AS) and the retreating side (RS) in all the joints. For the joints using the flat, convex, and concave shoulders 10 mm in diameter, the hook defects extended upward toward the top surface of the joints as shown in Fig. 2a–c. However, for the joints using the concave shoulder with diameters of 8 and 12 mm, the hook defects on both sides extended upward toward the keyhole periphery as shown in Fig. 2d, e.

Figures 3 and 4 show the typical fracture locations and tensile-shear loads of the FSSW AZ31 joints using different shoulders. It is found that the fracture of all the joints occurred along the orientation of the hook regions. The joint using the convex shoulder 10 mm in diameter exhibited the lowest tensile-shear load in the three joints. In addition, the load of the joints using the concave shoulders with diameters of 8, 10, and 12 mm increased with the increase in shoulder size.

Cross section and properties of FSSW AZ31 joints with the addition of Zn interlayer

Figure 5a shows the typical cross section photograph of the FSSW AZ31 joint with the addition of a 0.04-mm-thick Zn interlayer. At the keyhole periphery, the obvious reaction zone, marked with the letter A, was formed. At the same time, the hook defect was displaced by a thin strip composed of Mg–Zn intermetallics (Fig. 5b, c). In addition, a new Mg–Zn intermetallics brazed zone was formed (Fig. 5a, b), indicating that a good bond was obtained in place of the unbonded zone of the joint without the addition

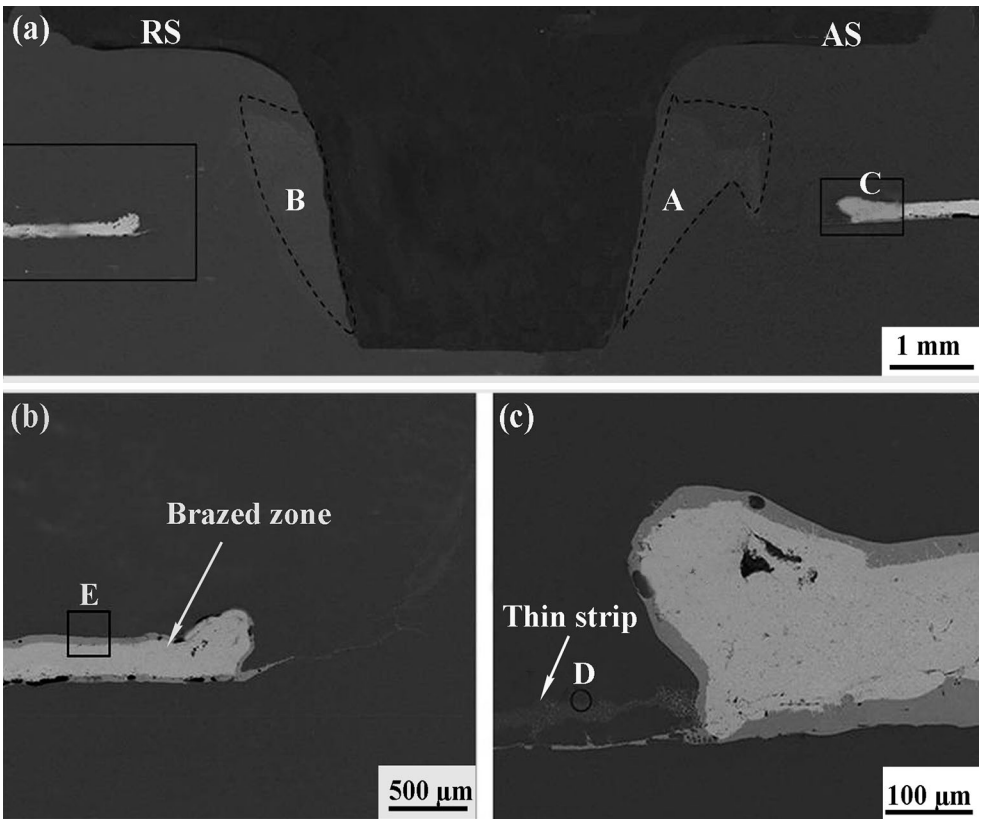

Fig. 7 **a** Typical cross-section photograph of FSSW AZ31 joint with an addition of 0.12-mm-thick Zn interlayer and the microstructures of **b** region B and **c** region C

of the Zn interlayer (Fig. 2). However, pores approximately 200 μm in diameter were detected on the AS and RS between the thin strip and brazed zone in the joint, which can be attributed to the intense diffusion reaction between the Mg substrate and the Zn interlayer (Fig. 5b, c).

Figure 6a shows the typical cross-section photograph of the FSSW AZ31 joint with the addition of a 0.08-mm-thick Zn interlayer. Similar to the joint with the addition of a 0.04-mm-thick Zn interlayer, the obvious reaction zone (region A) appeared at the keyhole periphery and the hook defect was eliminated by the formation of Mg–Zn intermetallics thin strip (Fig. 6b, c). It is noted that with the increasing interlayer thickness, the defect on the RS between the thin strip and brazed zone was decreased (Figs. 5b, 6b).

Figure 7a shows the typical cross-section photograph of the FSSW AZ31 joint with the addition of a 0.12-mm-thick Zn interlayer. The reaction zone (region A) was detected at the keyhole periphery similar to those in the above two joints. In addition, it is obvious that with further increase in the interlayer thickness, the joint quality was further improved due to the significant decrease of weld defects on the AS and RS between the thin strip and brazed zone as shown in Fig. 7b, c.

Figure 8a shows the typical cross-section photograph of the FSSW AZ31 joint with the addition of a 0.16-mm-thick Zn interlayer. With further increase in the interlayer thickness, the defects in the interface zone between the Mg substrate and the Zn interlayer almost disappeared (Fig. 8b, c). At the same time, the hook defect was eliminated, but the width and length of the thin strip composed of Mg–Zn intermetallics increased significantly in the hook region compared to those in the above three joints (Fig. 8c).

Figures 9 and 10 show the typical fracture locations and tensile–shear loads of the FSSW AZ31 joints produced using Zn interlayers with different thicknesses. It could be seen that fracturing of all the joints occurred along the Mg–Zn intermetallics layer. With the increase in the interlayer thickness, the load first increased and then decreased. When the interlayer thickness is 0.12 mm, the maximum load of the joint reaches 5.2 kN, which is far higher than that of the joint without the addition of the Zn interlayer. This indicates that the load of the FSSW AZ31 joints could be improved significantly by the addition of the Zn interlayer.

Microstructure and phase of FSSW AZ31 joints with the addition of Zn interlayer

In order to reveal the effect of the addition of the Zn interlayer on the microstructure and phase composition of

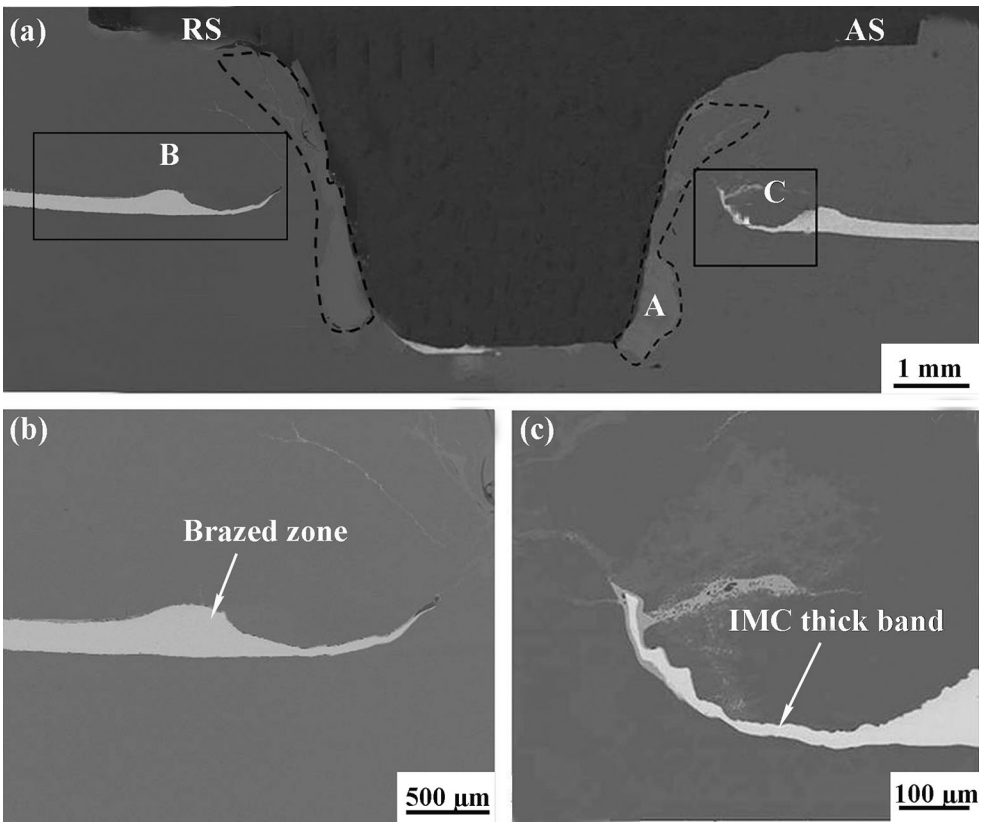

Fig. 8 **a** Typical cross-section photograph of FSSW AZ31 joint with an addition of 0.16-mm-thick Zn interlayer and the microstructures of **b** region B and **c** region C

the FSSW AZ31 joints, the joint with the 0.12-mm-thick Zn interlayer, which exhibited the highest load, was further investigated.

Figure 11a shows the typical magnified microstructure in region A of Fig. 7a. It can be found that an obvious reaction zone formed in this region at the keyhole periphery due to the reaction between Mg substrate and the broken Zn interlayer. The microstructure and composition of the reaction zone was further investigated by TEM. The results showed that a few small precipitates were distributed in this zone (Fig. 11b). EDS analysis revealed that the zone had a composition of 91.3at.% Mg and 8.7 at.% Zn (Fig. 11c) and was therefore assumed to be α-Mg phase with some small Mg–Zn precipitates.

The typical magnified microstructure of the thin strip in region D of Fig. 7c is shown in Fig. 12a. An obvious transition zone was detected between the AZ31 substrate and the thin strip. In the transition zone, lamellar structures (region C I in Fig. 12a) with compositions of about 72.3 at.% Mg and 27.7at.% Zn (Fig. 12c) were distributed between dark gray particles (region D in Fig. 12a), which were determined by EDS analysis to be the α-Mg phase, with compositions of 93.5 at.% Mg and 6.5 at.% Zn (Fig. 12d). In addition, the thin strip was composed of lamellar structure with compositions similar to those at the transition zone, based on EDS analysis.

In order to identify the microstructure and phases of the lamellar structures, the transition zone was further analyzed by TEM. Region E, as shown in Fig. 12b, with compositions of 49.5 at.% Mg and 50.5 at.% Zn (Fig. 12e), may be MgZn, and this is further validated by selected area electron diffraction (insert in Fig. 12b). In addition, region F, as shown in Fig. 12b, with compositions of 93.7 at.% Mg and 6.3 at.% Zn (Fig. 12f), may be α-Mg phase. Therefore, it could be determined that the thin strip was composed of a (α-Mg + MgZn) eutectoid structure, based on the EDS analysis, TEM observation, and the Mg–Zn phase diagram [26].

The typical magnified microstructure of region E in the brazed zone of Fig. 7b is shown in Fig. 13. The Mg substrate and Zn interlayer formed a sound brazed bonding in this zone (Fig. 13a). Adjacent to the Mg side, a eutectoid structure composed of α-Mg + MgZn was formed similar to that of the thin strip in Fig. 12, and next to the eutectoid structure, a reaction layer about 3-μm thick composed of Mg_7Zn_3 was detected (Fig. 13b). At the center of the brazed zone, there was another reaction zone as shown in Fig. 13c. EDS analysis showed that the bright zone was

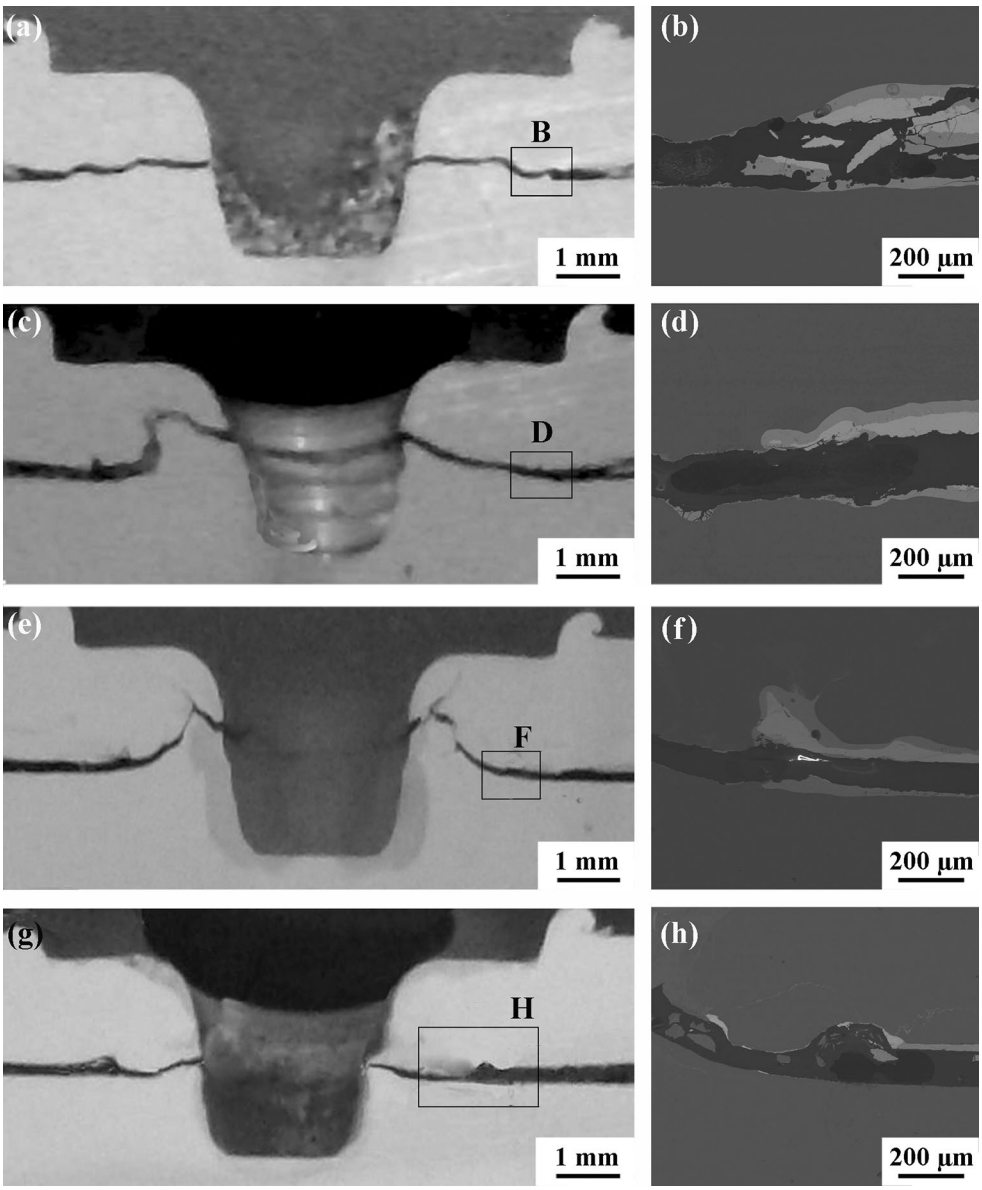

Fig. 9 **a**, **c**, **e**, **g** Typical fracture locations and **b**, **d**, **f**, **h** magnified photographs of FSSW AZ31 joints with addition of different thick Zn interlayers: **a**, **b** 0.04, **c**, **d** 0.08, **e**, **f** 0.12, and **g**, **h** 0.16 mm

residual Zn and the gray zone, with a composition of 35.6 at.% Mg and 64.4 at.% Zn, might be Mg_4Zn_7.

The microstructure and phase at the interface of the brazed zone were further identified by TEM. Figure 14a shows the TEM microstructure of the interface adjacent to the Mg side. It was further proven that the microstructure was α-Mg and (α-Mg + MgZn) eutectoid structure in this zone. Figure 14b shows the TEM microstructure of the zone next to the eutectoid structure. EDS analysis showed that the dark phase with a composition of 71.2 at.% Mg and 28.8 at.% Zn (Fig. 14b) should be Mg_7Zn_3. Figure 14c and d shows the TEM microstructure and the selected area electron diffraction pattern at the center of brazed zone. It can be seen that this zone was composed of Mg_4Zn_7 (also known as Mg_2Zn_3) [27] and unreacted Zn.

Discussion

Influence of Zn interlayers on the microstructure evolution of FSSW joints

During AZ31 FSSW with the addition of the Zn interlayer, the microstructure and phases of welded joints was closely related to the reaction between the Zn interlayer and the Mg substrate under the action of a stir tool. On the one

hand, the Zn interlayer of various zones had different reactions with the Mg substrate due to the differences in material flow and heat input; on the other hand, the thickness of the Zn interlayer would also influence the reaction extent between Zn and Mg, thereby influencing the microstructure of joints.

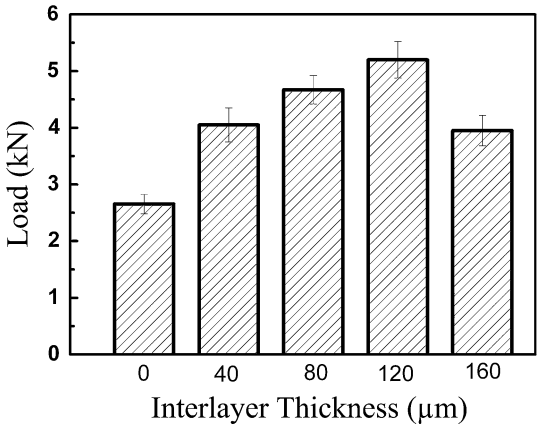

Fig. 10 Tensile load of FSSW AZ31 joints prepared using 10-mm-diameter concave shoulder with addition of different thick Zn interlayers

The Zn interlayer underneath the stir pin was broken first and then moved toward the pin root together with the Mg substrate underneath the shoulder, which had been heated and softened due to the action of the stir tool. Subsequently, the reaction between the broken Zn interlayer and the Mg substrate occurred at the keyhole periphery (Figs. 5a, 6a, 7a, 8a), forming the α-Mg phase with some small Mg–Zn precipitates (Fig. 11b).

The Zn interlayer underneath the shoulder can be divided into two zones. In the zone adjacent to the keyhole, the Zn interlayer was heated and softened, and then moved upward together with the Mg substrate. At the same time, the diffusion reaction between the extended Zn interlayer and the Mg substrate occurred in this zone (Figs. 5b, 6b, 7b, 8b). Therefore, the interlayer thickness had a significant effect on the extent of reaction between them. When the thickness of the interlayer was appropriate, the Zn would react completely with the Mg substrate to form the thin strip composed of the (α-Mg + MgZn) eutectoid structure (Fig. 12). This was the case for the joints with the addition of 0.04-, 0.08-, and 0.12-mm-thick Zn interlayers (Figs. 5c, 6c, 7c). However, when the interlayer was too thick, the Zn would react with the Mg to form a thick band composed of Mg–Zn intermetallics in the hook region of the FSSW

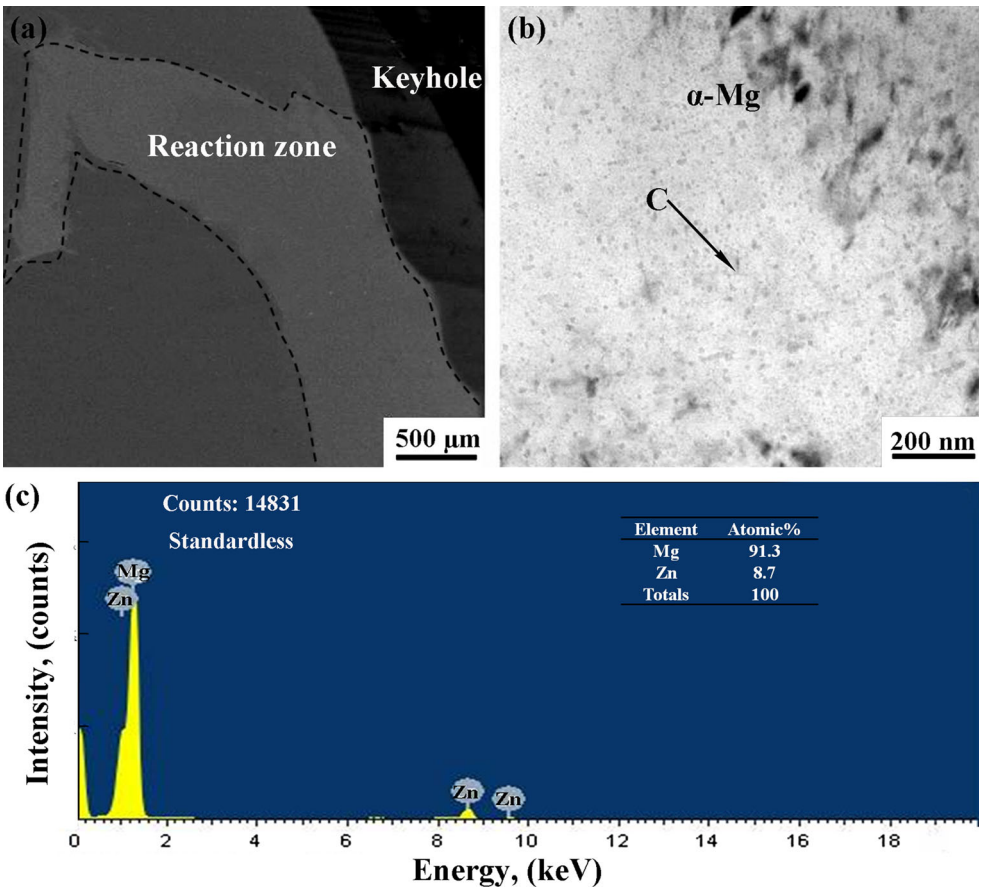

Fig. 11 **a** Magnified microstructure of region A in Fig. 7a, **b** typical TEM microstructure of reaction zone in **a**; **c** EDS spectrum obtained from zone C in **b**

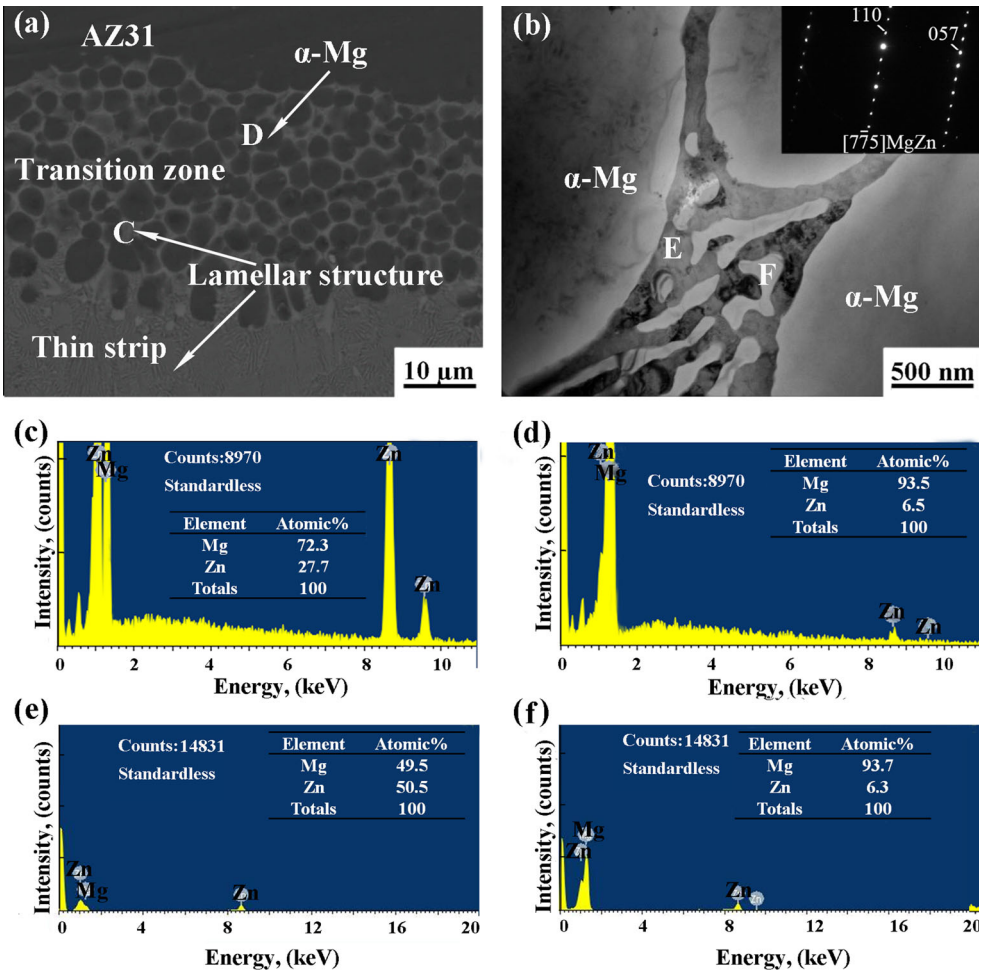

Fig. 12 **a** SEM microstructure of region D in Fig. 7b and **b** TEM microstructure of transition zone in **a**; EDS spectra obtained from regions, **c** C and **d** D in **a**, and regions, **e** E and **f** F in Fig. 12b

joint, which was the case for the joint with the addition of 0.16-mm-thick Zn interlayers (Fig. 8c).

In the zone under the edge of the shoulder, the Zn interlayer almost did not move, but could form a brazed bonding with the Mg substrate as shown in Figs. 5b, 6b, 7b, 8b. The brazed zone was mainly affected by the heat and pressure produced by the stir tool, so the interlayer thickness was one of the key factors affecting the quality of this zone at similar welding parameters. During FSSW, the Zn interlayer with a suitable thickness could react with the Mg substrate to form a good bonding zone composed of complex Mg–Zn intermetallics as shown in Fig. 7c. However, when the interlayer was too thin, it would result in the excessive diffusion reaction between the Mg substrate and the Zn interlayer and cause the occurrence of defects between the thin strip and the brazed zone, as shown in Figs. 5c, 6c.

According to the above analysis, a schematic of the microstructure evolution of the joints with the Zn interlayers is provided in Fig. 15. Under the action of the plunge, rotation, and keeping (dwell time) of the stir tool, the joint could be divided mainly into three typical parts, i.e., zones I, II, and III as shown in Fig. 15a and b.

In zone I, on one hand, the reaction temperature was higher than that in other zones; on the other hand, the broken Zn interlayer increased the contact area with the Mg substrate in the diffusion reaction as shown in Fig. 15c–e. Therefore, the Zn interlayer could diffuse completely into the Mg substrate during FSSW. During the cooling period, the transformation of L → α-Mg occurred. With a further decrease in temperature, a few small MgZn phases precipitated from the α-Mg.

In zone II, the Zn interlayer and Mg substrate could diffuse into each other. With the decrease in temperature, Mg_7Zn_3 phase was formed by the eutectic reaction of L → α-Mg + Mg_7Zn_3 at 340 °C. Then, with further decrease in temperature, some MgZn phases were eventually generated by the eutectoid reaction of Mg_7Zn_3 → α-Mg + MgZn at 325 °C. At last, a eutectoid microstructure composed of α-Mg and MgZn was formed in this zone. Therefore, the thin strip was composed of the (α-Mg + MgZn) eutectoid structure (Fig. 15c, d). However,

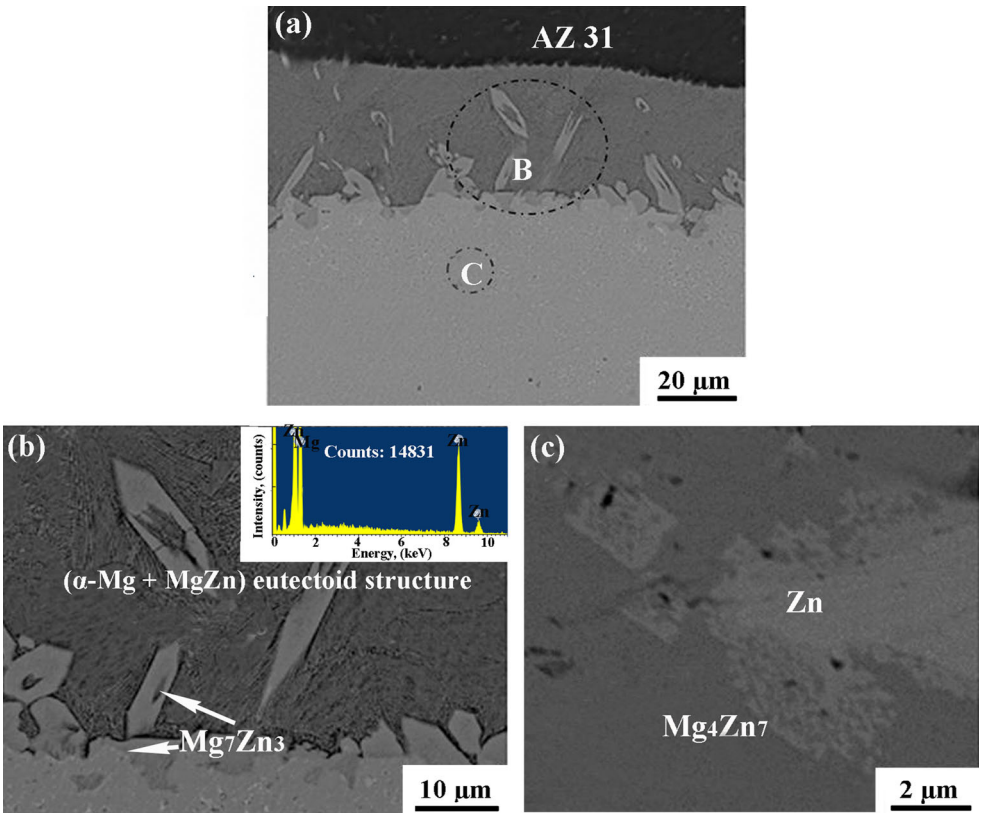

Fig. 13 **a** SEM microstructure of interface zone in region E of Fig. 7c and the microstructures of **b** region B and **c** region C

when the interlayer was too thick, Zn would also react with Mg to form a thick band composed of Mg–Zn intermetallics (Fig. 15e).

In zone III, adjacent to the Mg side, the eutectoid structure composed of α-Mg + MgZn was formed as shown in Fig. 15a. The reaction process is similar to that in zone II. Next to the eutectoid structure, the transition layer composed of Mg_7Zn_3 was detected. It is important to note that the phase diagram is obtained under the equilibrium state, and therefore inadequate to represent the rapid thermal changes taking place during FSSW. For the transition zone adjacent to the Zn interlayer, some Mg_7Zn_3 phases were in the remainder of the first eutectic structure, which did not turn into the final eutectoid structure in time during the rapid cooling period. At the center of the brazed zone, the content of Zn was much higher than that of Mg, therefore Zn could react with the Mg that diffused into the interlayer to form Mg_4Zn_7. In addition, the unreacted Zn remained after FSSW.

Based on the above observations, it can be concluded that the alloying process between the Zn interlayer and the Mg alloy substrate involved a complex phase transformation reaction and formed a variety of Mg–Zn intermetallic compounds.

Relationship between microstructure and mechanical properties

For the FSSW AZ31 joints without the addition of Zn interlayer, the crack initiated from the hook defect and failed once it grew from the tip of the hook to the nearest free surface in tensile-shear testing (Fig. 3). Therefore, the fracture direction and tensile-shear load of the FSSW joints were closely related to the orientation of the hook and the distance from the hook extremity to the nearest free surface. In this work, the width between the hook extremity and the keyhole periphery is defined as the effective welding spot width (EWSW), and the height between the hook extremity and the top surface of the weld is defined as the effective sheet thickness (EST). The measured EWSW and EST values on both AS and RS are listed in Table 1.

For the joints using the flat, convex, and concave shoulders 10 mm in diameter, the fracture was determined by the EST values according to the fracture location as shown in Fig. 3a–c. The joint using the convex shoulder had a lower value than those using the flat and concave shoulders (Table 1), and therefore exhibited the lowest tensile-shear load of the three joints (Fig. 4).

For the joints using concave shoulders with diameters of 8 and 12 mm, the fracture was determined by the EWSW

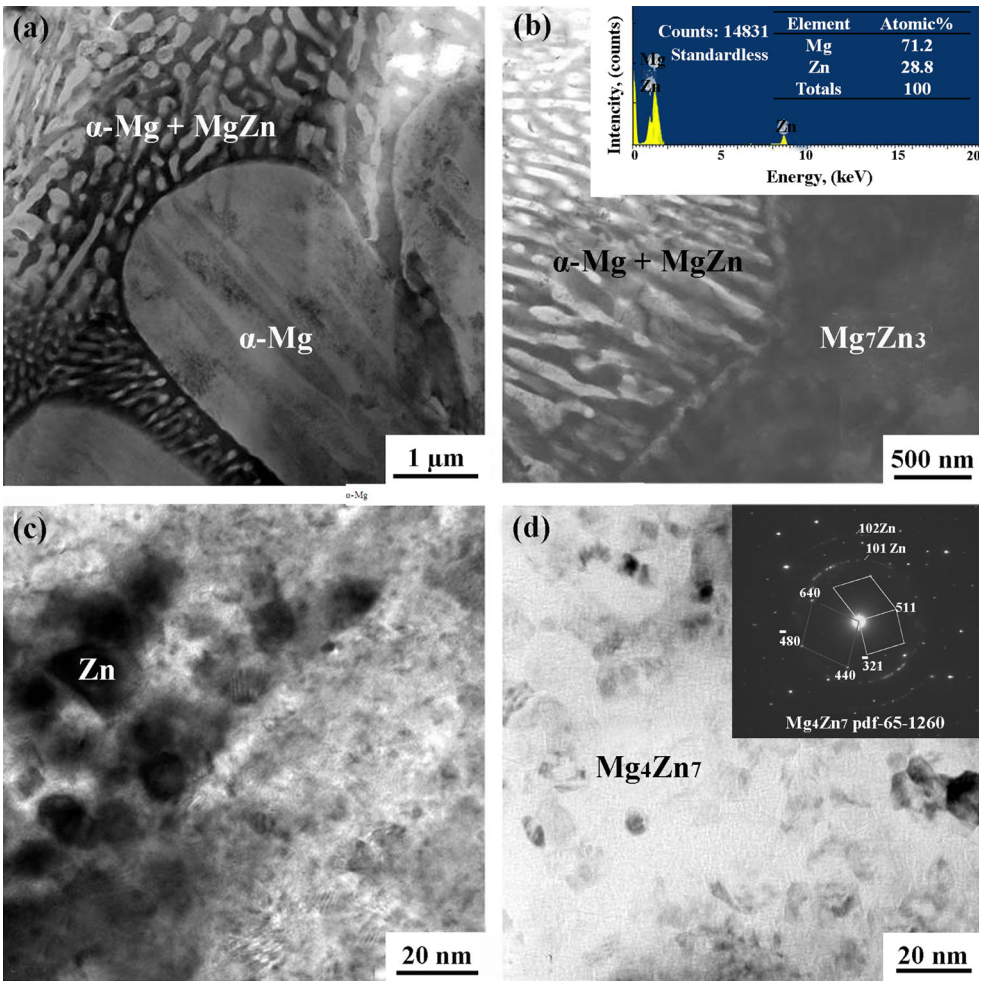

Fig. 14 TEM images showing interfacial microstructures: **a** adjacent to the Mg side and **b** next to eutectoid structure; **c** TEM microstructure at the center of brazed zone and **d** its selected area electron diffraction pattern

value (Fig. 3d, e). The EWSW value of the former joint is less than the latter, so the load of the former joint is lower than that of the latter one (Fig. 4). In addition, the EWSW value in the joint using the concave shoulder with the diameter of 12 mm is greater than the EST value in the joints using the flat, convex, and concave shoulders 10 mm in diameter, so the load of the joint using 12-mm-diameter concave shoulder is the greatest as shown in Fig. 4 and Table 1.

It is clear that increasing the distance from the hook extremity to the nearest free surface is beneficial to increasing the load of the joints. The variation of shoulder shape and size could change the hook character, but could not eliminate the hook defects.

For the FSSW AZ31 joints with the addition of Zn interlayers, the Zn interlayer promoted the formation of Mg–Zn brazed zone (zone III) and eliminated the hook defects (Figs. 5, 6, 7). In tensile-shear testing, the fracture initiated from the intermetallics rather than the hook defects, and then a crack propagated along the Mg–Zn strip composed of (α-Mg + MgZn) eutectoid structure (zone II). At last, joints fractured through the reaction zone at the keyhole periphery (zone I) as shown in Fig. 9. Therefore, the formation of the brazed zone (zone III) composed of Mg–Zn intermetallics significantly increased the area of the bonded zone of the joints, thereby increasing the joint load as shown in Figs. 4 and 10. In addition, the joints fractured through the Mg–Zn intermetallics zone (Figs. 9b, d, f, h), indicating that the strength of the intermetallics is lower than that of the Mg alloy.

For the joint with the addition of the 0.12-mm-thick Zn interlayer, a Mg–Zn brazed zone with few defects formed to increase significantly the area of the bonded zone of the joint (Fig. 7), while the hook defect was replaced by the thin strip composed of the (α-Mg + MgZn) eutectoid structure (Figs. 12, 13, 14). Therefore, the joint exhibited the highest load (Fig. 10). For the joints with the addition of the 0.04- and 0.08-mm-thick Zn interlayers, defects between the thin strip and the brazed zone were detected (Figs. 5c, 6c), influencing the load of the joints. For the joint with the addition of the 0.16-mm thick Zn interlayer, the formation of a long and thick band composed of

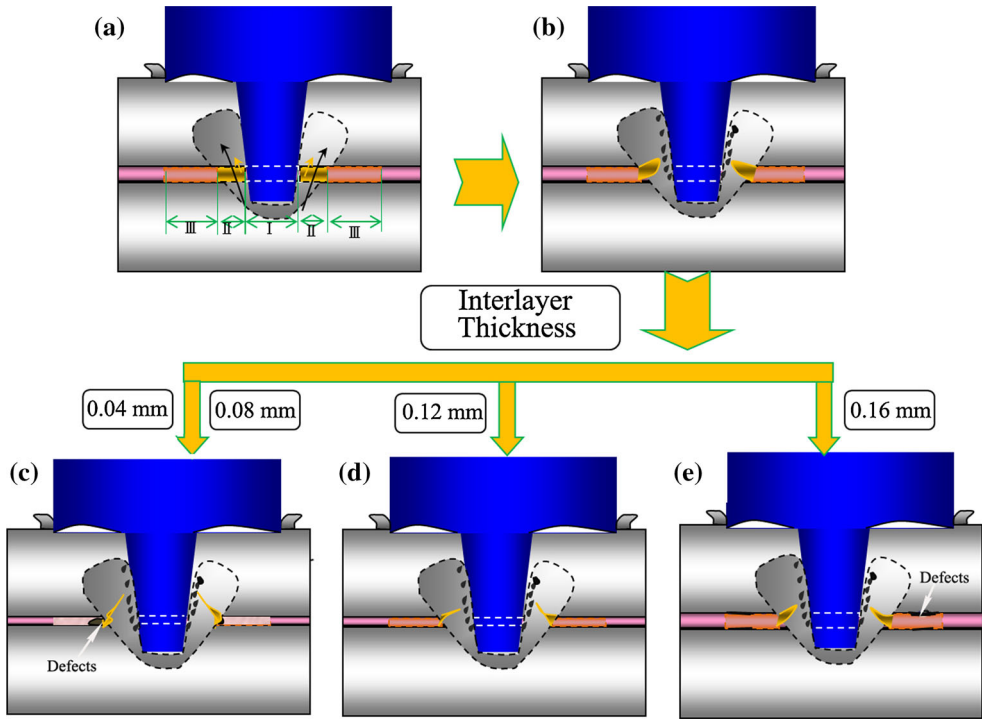

Fig. 15 Schematic of microstructure evolution of typical FSSW joints: **a** three zones of Zn interlayer, **b** movement of Zn interlayer in three zones; microstructure character of joints with the addition of **c** 0.04- and 0.08-mm, **d** 0.12-mm, and **e** 0.16-mm-thick Zn interlayers

Table 1 Summary of fraction location, effective welding spot width (EWSW), and effective sheet thickness (EST) values

Joints	Shoulder		AS (mm)		RS (mm)		Fracture location
	End surface	Size (mm)	EWSW	EST	EWSW	EST	
1	Flat	Φ10	2.0	0.5	2.5	1.1	From the hook tip to the top surface
2	Convex	Φ10	1.4	0.4	1.5	0.6	From the hook tip to the top surface
3	Concave	Φ10	2.2	0.8	2.3	0.7	From the hook tip to the top surface
4	Concave	Φ8	0.8	1.1	1.2	1.2	From the hook tip to the keyhole
5	Concave	Φ12	2.0	0.8	1.5	0.8	From the hook tip to the keyhole

Mg–Zn intermetallics with low strength was not beneficial to the increase of the joint load (Fig. 8c). As a result, with the increase in the interlayer thickness, the load first increased and then decreased.

Conclusions

In this study, the effects of adding different thick Zn interlayers on the microstructural features and properties of FSSW AZ31 joints were investigated. The following conclusions were drawn.

(1) For the FSSW joints without the addition of Zn interlayer, although the loads of the joints could be increased by changing the end surface geometry and the size of the shoulders, the small bonded area and hook defect limited further increase of the joint loads. The joint with the 12-mm-diameter concave shoulder exhibited the greatest tensile-shear load of about 3.5 kN.

(2) Adding the Zn interlayer with a suitable thickness could lead to the formation of a brazed zone composed of complex Mg–Zn intermetallics and a thin strip of (α-Mg + MgZn) eutectoid structure in the FSSW joints, to replace the unbonded zone and hook region in the FSSW joints without the Zn interlayer, thereby increasing the area of the bonded zone and eliminating the hook defects at the same time.

(3) When the interlayer was too thick, Zn would react with Mg to form a thick band composed of Mg–Zn intermetallics in the hook region of FSSW joints. When the interlayer was too thin, it would result in the excessive diffusion reaction between the Mg substrate and the Zn interlayer and cause the occurrence of more defects between the thin strip and the brazed zone.

(4) For the joints with the addition of the Zn interlayer, with the increase in interlayer thickness, tensile-shear loads of the joints first increased and then

decreased. When the interlayer thickness was 0.12 mm, the maximum load of the joints could reach 5.2 kN, which is far higher than that of the joint using the same shoulder without the addition of the Zn interlayer (about 2.5 kN).

Acknowledgments This study was supported by the National R&D Program of China under Grant No. 2011BAE22B05, and the National Natural Science Foundation of China under Grant Nos. 51371179 and 51331008.

References

1. Lathabai S, Painter MJ, Cantin GMD, Tyagi VK (2006) Friction spot joining of an extruded Al-Mg-Si alloy. Scripta Mater 55:899
2. Gerlich A, Su P, North TH (2005) Tool penetration during friction stir spot welding of Al and Mg alloys. J Mater Sci 40:6473. doi:10.1007/s10853-005-1568-9
3. Bilici MK, Yukler AI, Kurtulmus M (2011) The optimization of welding parameters for friction stir spot welding of high density polyethylene sheets. Mater Des 32:4074
4. Rodrigues DM, Loureiro A, Leitao C (2009) Influence of friction stir welding parameters on the microstructural and mechanical properties of AA6016-T4 thin welds. Mater Des 30:1913
5. Patel VK, Bhole SD, Chen DL (2011) Influence of ultrasonic spot welding on microstructure in a magnesium alloy. Scripta Mater 65:911
6. Gerlich A, Su P, North TH (2005) Friction stir spot welding of Mg-alloys for automotive. In: Neelameggham NR, Kaplan HI, Powell BR (eds) Magnesium technology. TMS, Warrendale, pp 383–388
7. Rao HM, Jordon JB, Barkey ME, Guo YB, Su XM, Badarinarayan H (2013) Influence of structural integrity on fatigue behavior of friction stir spot welded AZ31 Mg alloy. Mater Sci Eng A 564:369
8. Yin YH, Sun N, North TH, Hu SS (2010) Hook formation and mechanical properties in AZ31 friction stir spot welds. J Mater Process Technol 210:2062
9. Su P, Gerlich A, North TH, Bendzsak GJ (2006) Material flow during friction stir spot welding. Sci Technol Weld Join 11:61
10. Gerlich A, Su P, Yamamoto M, North TH (2008) Material flow and intermixing during dissimilar friction stir welding. Sci Technol Weld Join 13:254
11. Su P, Gerlich A, North TH, Bendzsak GJ (2007) Intermixing in dissimilar friction stir spot welds. Metall Mater Trans A 38:584
12. Yuan W, Mishra RS, Carlson B, Verma R, Mishra RK (2012) Material flow and micro structural evolution during friction stir spot welding of AZ31 magnesium alloy. Mater Sci Eng A 543:200
13. Yin YH, Sun N, North TH, Hu SS (2010) Microstructures and mechanical properties in dissimilar AZ91/AZ31 spot welds. Mater Charact 61:1018
14. Yin YH, Sun N, North TH, Hu SS (2010) Influence of tool design on mechanical properties of AZ31 friction stir spot welds. Sci Technol Weld Join 15:81
15. Horie S, Shinozaki K, Yamamoto M, Kadoi K, Nakanshin H, North TH (2010) Effects of tool geometry and process conditions on material flow and strength of friction stir spot welded joints. Transact JWRI 39:28
16. Zhang YN, Cao X, Larose S, Wanjara P (2012) Review of tools for friction stir welding and processing. Can Metall Q 51:250
17. Ni YQ (2012) Study on the bonding-friction stir spot hybrid welding procedure of AZ31 Mg alloy. Dalian Jiaotong University, Dalian
18. Shen J, Min D, Wang D (2011) Effects of heating process on the microstructures and tensile properties of friction stir spot welded AZ31 magnesium alloy plates. Mater Des 32:5033
19. Dhanapal A, Boopathy SR, Balasubramanian V (2011) Developing an empirical relationship to predict the corrosion rate of friction stir welded AZ61 magnesium alloy under salt fog environment. Mater Des 32:5066
20. Wang DA, Lee SC (2007) Microstructures and failure mechanisms of friction stir spot welds of aluminum 6061-T6 sheets. J Mater Process Technol 186:291
21. Lathabai S, Painter MJ, Cantin GMD, Tyagi VK (2006) Friction spot joining of anextruded Al-Mg-Si alloy. Scripta Mater 55:899
22. Bozzil S, Etter AL, Baudin T, Klosek V, Kerbiguet JG, Criqui B (2010) Influence of FSSW parameters on fracture mechanisms of 5182 aluminium welds. J Mater Process Technol 210:1429
23. Liu LM, Wu ZH (2010) Microstructure and interfacial reactions of soldering magnesium alloy AZ31B. Mater Charact 61:13
24. Ma L, Long WM, Qiao PX, He DY, Li XY (2013) Development of a binary Zn-based solder alloy for joining wrought magnesium alloy AZ31B. J Mater Eng Perform 22:118
25. Wu H, Song G (2010) Microstructure and properties of brazing joints of magnesium alloy AZ31B. Mater Res Innov 14:160
26. Clark JB, Zabdyr L, Moser Z (1998) In: Nayebhashemi AA, Clark JB (eds) Phase diagrams of binary magnesium alloys. ASM International, Metals Park p353
27. Ni JF (2012) Precipitation and hardening in magnesium alloys metal. Metall Mater Trans A 43:3891